

Article

## Pt Monolayer Shell on Nitrided Alloy Core—A Path to Highly Stable Oxygen Reduction Catalyst

Jue Hu <sup>1,2</sup>, Kurian A. Kuttiyiel <sup>1</sup>, Kotaro Sasaki <sup>1,\*</sup>, Dong Su <sup>1</sup>, Tae-Hyun Yang <sup>3</sup>, Gu-Gon Park <sup>3,\*</sup>, Chengxu Zhang <sup>2</sup>, Guangyu Chen <sup>1</sup> and Radoslav R. Adzic <sup>1,\*</sup>

<sup>1</sup> Chemistry Department, Brookhaven National Laboratory, Upton, NY 11973, USA; E-Mails: juehu@bnl.gov (J.H.); kurian@bnl.gov (K.A.K.); dsu@bnl.gov (D.S.); chgyhit@gmail.com (G.C.)

<sup>2</sup> Hefei Institutes of Physical Science, Chinese Academy of Sciences, P.O. Box 1126, Hefei 230031, China; E-Mail: chxzhang@ipp.ac.cn

<sup>3</sup> Fuel Cell Research Center, Korea Institute of Energy Research, Daejeon 305-343, Korea; E-Mail: thyang@kier.re.kr

\* Authors to whom correspondence should be addressed; E-Mails: ksasaki@bnl.gov (K.S.); gugon@kier.re.kr (G.-G.P.); adzic@bnl.gov (R.R.A.); Tel.: +1-631-344-3446 (K.S.); +82-42-860-3782 (G.-G.P.); +1-631-344-4522 (R.R.A.); Fax: +1-631-344-5815 (R.R.A.).

Academic Editor: Minhua Shao

Received: 15 May 2015 / Accepted: 13 July 2015 / Published: 22 July 2015

---

**Abstract:** The inadequate activity and stability of Pt as a cathode catalyst under the severe operation conditions are the critical problems facing the application of the proton exchange membrane fuel cell (PEMFC). Here we report on a novel route to synthesize highly active and stable oxygen reduction catalysts by depositing Pt monolayer on a nitrided alloy core. The prepared Pt<sub>ML</sub>PdNiN/C catalyst retains 89% of the initial electrochemical surface area after 50,000 cycles between potentials 0.6 and 1.0 V. By correlating electron energy-loss spectroscopy and X-ray absorption spectroscopy analyses with electrochemical measurements, we found that the significant improvement of stability of the Pt<sub>ML</sub>PdNiN/C catalyst is caused by nitrogen doping while reducing the total precious metal loading.

**Keywords:** nickel nitride; ORR; electrocatalyst; core-shell; stability; Pt monolayer

---

## 1. Introduction

Proton exchange membrane fuel cell (PEMFC) is expected to be an alternative power-generation for vehicles, stationary, and portable power applications because of its high energy density, low operation temperature, low air pollution and the use of renewable fuels, such as hydrogen and some alcohol [1,2]. Although the PEMFC power source technique has been really influential in the last decade, the slow kinetics of the oxygen reduction reaction (ORR) is still one of the main obstacles hampering the large scale applications of PEMFC [3]. Platinum (Pt) as the most effective catalyst for ORR has been the general choice. However, high Pt loading at the cathode as well as inadequate activity and stability of Pt under severe operation conditions are still unresolved problems facing the PEMFC [4,5]. To overcome these problems, it is essential to decrease the Pt amount in electrocatalysts, and at the same time, improve the performance of the Pt-based cathode catalyst both in terms of activity and stability. To this end, one of the strategies is to develop the metal@Pt core-shell structure catalysts in which a non-Pt core is employed and covered by atomically thin layers of Pt. This core-shell structure allows efficient use of Pt, and thereby can reduce the demands on Pt while enhancing the catalyst performance [6–9].

Significant progress has been made through the combination of experimental and theoretical studies [10,11]. We developed a new class of catalysts consisting of a Pt monolayer on different metals and alloy supporting cores, including Pd, Ru, Ir, Rh, Au, PdAu, IrNi, IrRe, and AuNiFe [12–18]. The ORR activity of Pt monolayer on different metal surfaces shows a volcano-type dependence on the d-band center of Pt [18]. The strain-induced d-band center shifts and electronic ligand effects between the substrate and the overlayer are the two main factors determining the activity of these core-shell catalysts [6]. Nevertheless, the improving the electrocatalytic activity and stability of Pt-based cathode catalysts simultaneously is still a challenge. Great efforts have been made to modify the Pt surface with other elements such as Au [19]. The oxidation of Pt on Au-modified Pt surfaces requires much higher potentials than that on unmodified Pt surface, resulting in the enhancement of the catalyst stability [19]. Another strategy is to modify the metal core. Gong *et al.* synthesized highly stable Pt<sub>ML</sub>AuNi<sub>0.5</sub>Fe catalysts and found that the Au shell in the core precluded the exposure of NiFe to the electrolyte leading to the high electrochemical stability [20]. Kuttiyiel *et al.* also developed a highly stable ORR catalyst by Au-stabilized PdNi [21]. More recently, we have reported a new approach to develop Pt-M (Ni, Co, and Fe) core-shell catalysts with high stability and activity by nitriding core metals [22,23]. The synchrotron XRD analysis proved the generation of the highly stable Fe<sub>4</sub>N, Co<sub>4</sub>N, and Ni<sub>4</sub>N nitride cores. Since the Pt monolayer on Pd core catalyst is on the top of the volcano plot as mentioned above, and also the price of Pd is considerably lower than that of Pt [24], we selected Pt monolayer on nitride stabilized PdNi core (Pt<sub>ML</sub>PdNiN) for studying its synthesis and structure in detail with the possibility to simultaneously improve its stability and activity, while reducing the PGM metal content.

## 2. Results and Discussion

PdNi alloy nanoparticles were first synthesized by chemical reduction (see experimental section), followed by thermal annealing in N<sub>2</sub> at 250 °C for 1 h, and subsequent annealing at 510 °C for 2 h in NH<sub>3</sub> as the nitrogen precursor. As illustrated in Figure 1, the PdNiN nanoparticles have a core-shell structure with Ni in the core and Pd on the surface. Figure 1a shows a high angle annular dark field

scanning transmission electron microscope (HAADF-STEM) image of a representative single PdNiN nanoparticle. Elementary characterization of the PdNiN nanoparticle was performed by the electron energy-loss spectroscopy (EELS) mapping for Pd (M-edge, 2122 eV) and Ni (L-edge, 855 eV) from the nanoparticle shown in Figure 1a. As shown in Figure 1b, overlapping the mapping of Pd and Ni EELS signal validates an obvious Ni-core and Pd-shell structure. However, the outside of the particle is decorated by a trace amount of Ni/Ni oxides. The Ni/Ni oxides would not affect the electrocatalytic activity of these particles because they quickly dissolve in acid conditions during the Pt monolayer deposition. Figure 1c and Figure S1 (Supplementary Information) shows a line profile analysis by STEM-EELS illustrating the distribution of the Pd and Ni components in a single representative nanoparticle. It is evident that the Pd atoms are distributed uniformly over the Ni; the Pd shell thickness is determined to be around 0.6–1.5 nm by examining a number of particles. From the TEM images, the average particle size of the PdNiN nanoparticles was determined to be around 11 nm (Figure S2).

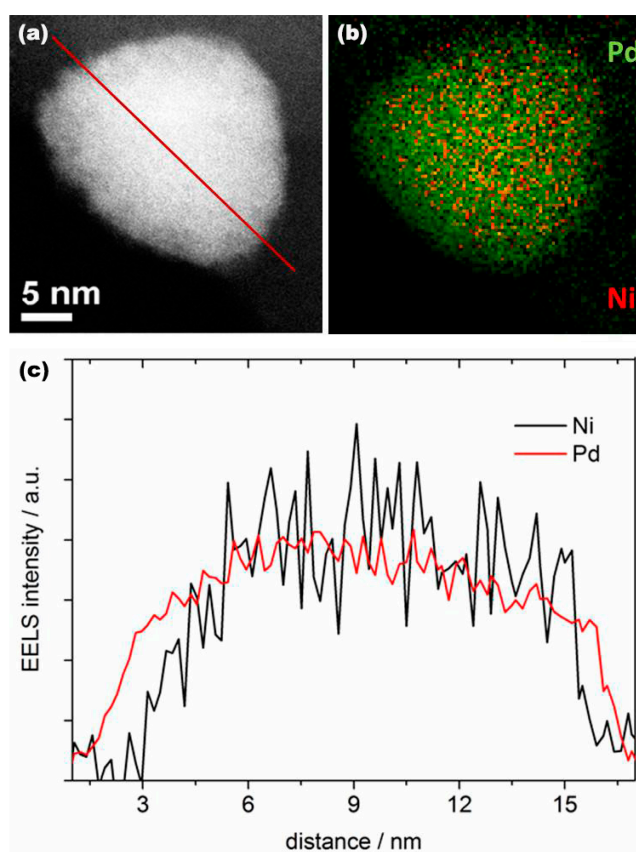


**Figure 1.** (a) HAADF-STEM image of PdNiN core-shell nanoparticle; (b) Two dimensional EELS mapping of Ni L signal (red) and Pd M signal (green) from a single nanoparticle; (c) EELS line scan profile for Pd M-edge and Ni L-edge along the scanned line indicated in (a).

To verify the formation of NiN<sub>x</sub> core in PdNiN nanoparticles we carried out X-ray absorption spectroscopy (XAS) measurements and compared the obtained spectra with those of reference metal foils, as shown in Figure 2. X-ray absorption near-edge structure (XANES) of Ni K edge from PdNiN nanoparticles shows that the electronic state of Ni has been changed due to the presence of N forming NiN<sub>x</sub> species. The Fourier transform (FT) magnitudes of the extended x-ray absorption fine structure (EXAFS) data for Ni-K edge (Figure 2c) for PdNiN presents a decrease in Ni bonding distance due to

the formation of Ni nitrides. Also previous studies have shown that EXAFS for NiO or Ni(OH)<sub>2</sub> species demonstrate a peak at 1.6 Å corresponding to the Ni–O bond, accompanied by small peak at around 2.4 Å corresponding to the Ni–Ni bond [25]. The absence of these peaks along with the changes in the bonding distance compared to Ni metal verifies the presences of N<sub>x</sub> species in the PdNiN. The alloying effect of PdNiN<sub>x</sub> has changed the electronic states of Pd as well, and these distinctions are clearly observed in the XANES and EXAFS regions when compared to those from a Pd foil (Figure 2b,d). The appearance of a peak around 2.0 Å in FT EXAFS of Pd K edge for PdNiN is likely caused by Pd–Ni bond. Although the exact species of NiN<sub>x</sub> could not be determined, the XAS results along with the STEM-EELS analysis indicate that Ni in the core-shell structured PdNiN nanoparticles is nitrated. Our previous studies on nitrated Pt–M (*M* = Ni, Fe or Co) core-shell nanoparticles have indicated the presences of M<sub>4</sub>N species [22,23]. As the synthesis parameters are similar to the previous study we presume the presence of Ni<sub>4</sub>N species in our PdNiN core-shell nanoparticles.

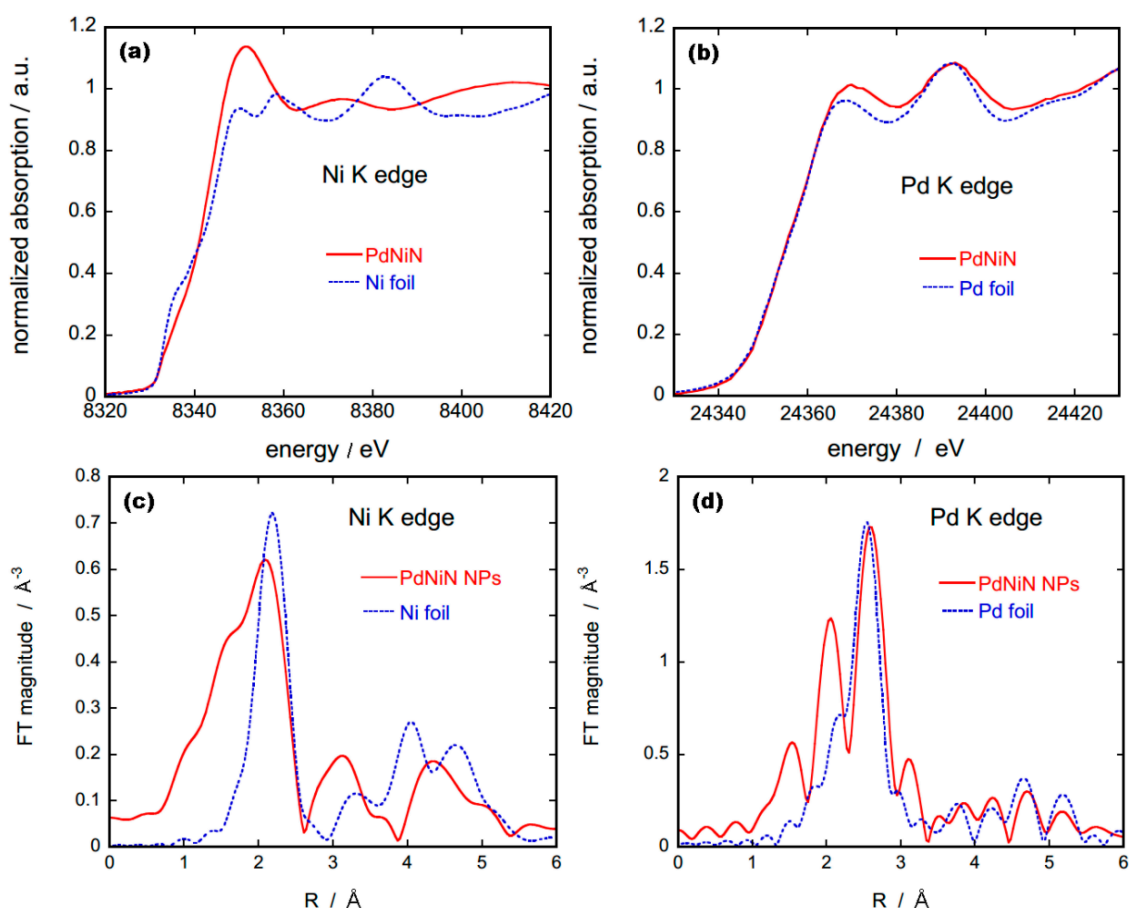


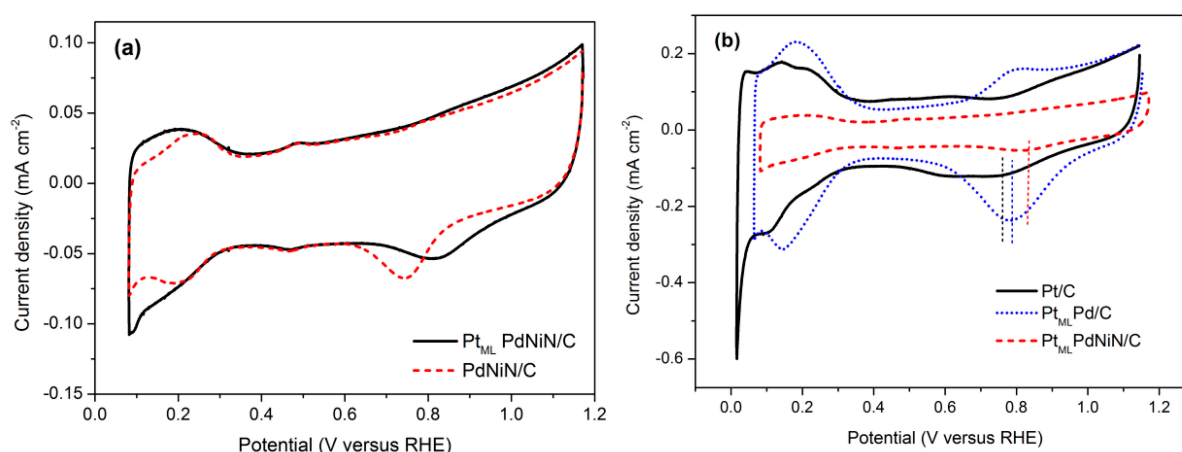
**Figure 2.** (a,b) Normalized XANES spectra for Ni and Pd K edges respectively along with Ni and Pd reference foil; (c,d) FT EXAFS spectra for Ni and Pd K edges respectively along with their reference foils.

The cyclic voltammetry (CV) curves obtained on the PdNiN/C and Pt<sub>ML</sub>PdNiN/C catalysts in Ar-saturated 0.1 M HClO<sub>4</sub> solution are shown in Figure 3a. It is observed that the curves in the hydrogen adsorption/desorption region of the Pt<sub>ML</sub>PdNiN/C resembled those of a typical Pt/C surface although the peaks from (110) and (100) planes are suppressed due to the interaction of the substrate materials. Moreover, after a Pt<sub>ML</sub> depositing on the PdNiN/C surface, the oxide adsorption/desorption potentials

shift more positively. The surface area of *i-E* plot associated with the hydrogen desorption can be used to estimate the electrochemical surface area (ECSA) of Pt catalysts. The ECSA of catalyst can be calculated according to Equation (1) [26]:

$$S_{\text{ECSA}} = \frac{Q_{\text{H}}}{L_{\text{Pt}} \times 0.21} \quad (1)$$

in which  $L_{\text{Pt}}$  represents the Pt loading ( $1.13 \mu\text{g}\cdot\text{cm}^{-2}$  derived from the Cu under-potential deposition charge),  $Q_{\text{H}}$  ( $\text{mC}\cdot\text{cm}^{-2}$ ) is the charge exchanged during the electro-desorption of hydrogen on Pt surface and  $0.21$  ( $\text{mC}\cdot\text{cm}^{-2}$ ) is the charge required to oxidize a monolayer of hydrogen on a smooth Pt [27]. The ECSA value of the catalyst is  $90 \text{ m}^2\cdot\text{g}^{-1}\text{Pt}$ . Comparison of CVs from the commercial Pt/C (E-TEK, 10 wt. %), Pt<sub>ML</sub> deposited commercial Pd/C (E-TEK, 10 wt. %, 3.5 nm Pd particle size) and Pt<sub>ML</sub>PdNiN/C catalysts (Figure 3b) showed that the oxide adsorption/desorption wave of Pt<sub>ML</sub>PdNiN/C occurred 37 mV and 60 mV positive compared to the Pt<sub>ML</sub>Pd/C and commercial Pt/C catalyst, respectively. The elevation of Pt oxidation potential on the Pt<sub>ML</sub>PdNiN/C catalyst indicates stabilization of the Pt<sub>ML</sub> on the PdNiN/C substrate [19].



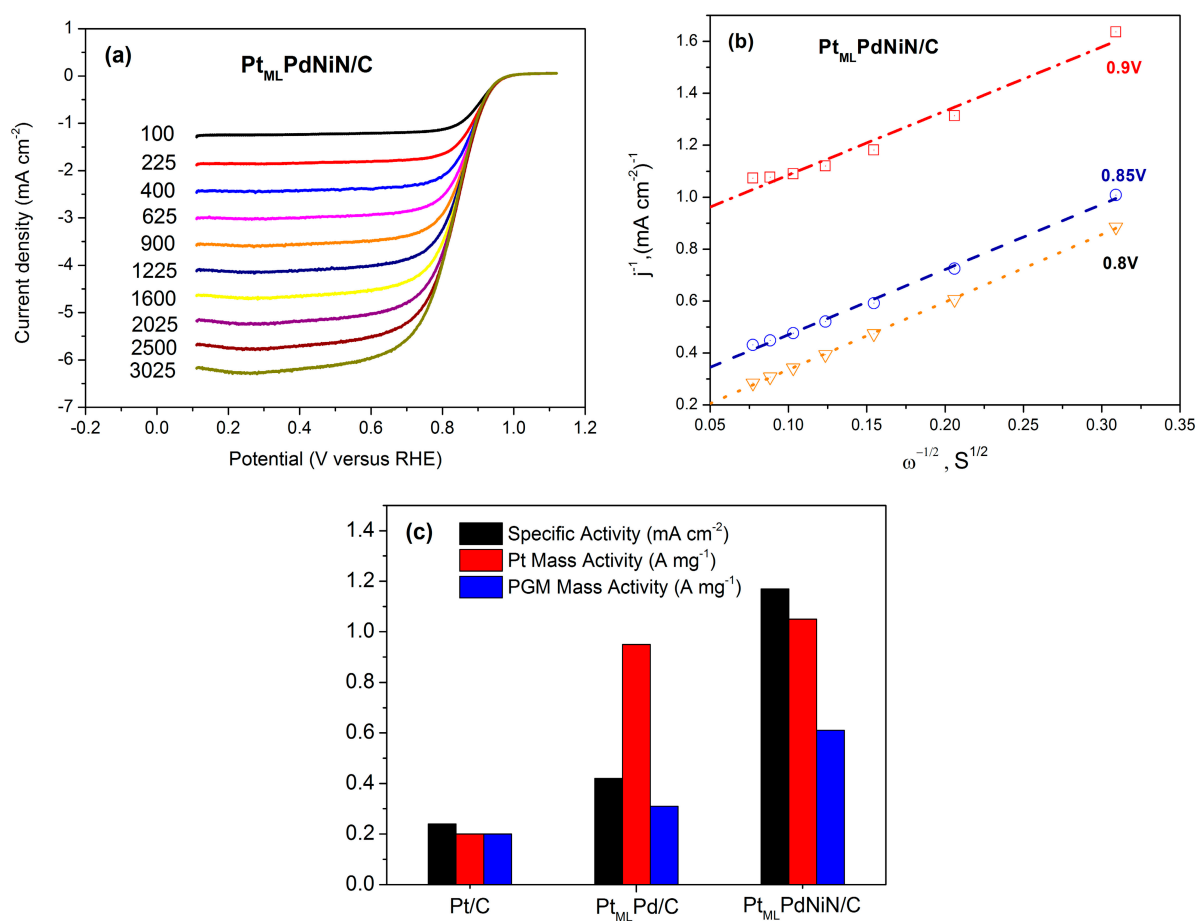
**Figure 3.** Cyclic voltammograms for (a) obtained PdNiN/C and Pt<sub>ML</sub>PdNiN/C; and (b) commercial Pt/C, Pt<sub>ML</sub>Pd/C and Pt<sub>ML</sub>PdNiN/C nanoparticles in 0.1 M HClO<sub>4</sub> solution at a scan rate of  $20 \text{ mV}\cdot\text{s}^{-1}$ .

Figure 4a shows rotating disk electrode (RDE) measurements of the ORR on the Pt<sub>ML</sub>PdNiN/C catalyst in O<sub>2</sub> saturated 0.1 M HClO<sub>4</sub> solution at a sweep rate of  $10 \text{ mV}\cdot\text{s}^{-1}$  and the rotation speeds from 100 to 3025 rpm. The high onset potential (*ca.* 1.0 V) and half-wave potential (850 mV at the rotation rate of 1600 rpm) of O<sub>2</sub> reduction at an ultra-low Pt loading ( $1.13 \mu\text{g}\cdot\text{cm}^{-2}$ ) indicate a good ORR activity of a Pt<sub>ML</sub>PdNiN/C catalyst. The kinetic current density  $j_k$  was calculated from these ORR polarization curves (Figure 4a) using the Koutecky-Levich equation [22]:

$$\frac{1}{j} = \frac{1}{j_k} + \frac{1}{B\omega^{1/2}} \quad (2)$$

where  $j$  is the measured current density,  $B$  and  $\omega$  are the constant and rotation rate, respectively. As can be seen from the Koutecky-Levich plot ( $1/j$  plotted as a function of  $\omega^{-1/2}$ ), shown in Figure 4b, the linearity and parallelism of the plots at 0.8 V, 0.85 V, and 0.9 V indicate the first-order kinetics with

respect to molecular oxygen [28]. The intercept with the y-axis gives the inverse kinetic current density. The specific activity was determined from the normalization of kinetic current density to the ECSA while the kinetic current density was normalized to the loading of Pt or platinum group metal (PGM) to calculate the mass activity. The specific activity of the Pt<sub>ML</sub>PdNiN/C catalyst is 1.17 mA·cm<sup>-2</sup> at 0.9 V, which is more than four times higher than that of commercial Pt/C catalyst (0.24 mA·cm<sup>-2</sup>), and 2.5 times higher than that of the commercial Pd/C with Pt monolayer (0.42 mA·cm<sup>-2</sup>). However, higher ORR activities for commercial Pt/C catalyst were observed in some literature [29,30]. The Pt mass activity of Pt<sub>ML</sub>PdNiN/C catalyst (1.05 A·mg<sup>-1</sup>) is more than five times higher than the commercial Pt/C catalyst (0.2 A·mg<sup>-1</sup>) and is also greater than the Pt<sub>ML</sub>Pd/C catalyst (0.95 A·mg<sup>-1</sup>) [21].



**Figure 4.** ORR polarization curves for the Pt<sub>ML</sub>PdNiN/C nanoparticles in 0.1 M HClO<sub>4</sub> solution at a scan rate of 10 mV·s<sup>-1</sup> at various rpm. (b) The Koutechy-Levich plots at 0.8 V, 0.85 V and 0.9 V obtained from the ORR polarization curves as shown in (a). (c) Specific and mass activities for the commercial Pt/C, Pt<sub>ML</sub>Pd/C and Pt<sub>ML</sub>PdNiN/C catalysts at 0.9 V.

In addition to the high electrochemical activities, the Pt<sub>ML</sub>PdNiN/C catalyst also exhibited excellent stability. The stability of the electrocatalyst was evaluated by an accelerated durability test involving potential cycling between 0.6 V and 1.0 V at the sweep rate of 50 mV·s<sup>-1</sup> using a RDE in an air-saturated 0.1 M HClO<sub>4</sub> solution at room temperature. Figure 5a shows the ORR polarization curves of the Pt<sub>ML</sub>PdNiN/C catalyst at 1600 rpm before and after 30,000 and 50,000 potential cycles. After 30,000 cycles, the half-wave potential of the ORR polarization curve remained at almost the initial value. After

50,000 cycles, the ORR measurements showed only 10 mV loss in the half-wave potential. This observation is similar to the previous results of Pt<sub>ML</sub>Pd/C nanoparticles that retained their ORR activity even after losing their electrochemical surface area (ECSA) [31]. This can be explained by the concept that the Pd dissolution in the catalyst induces contraction to the Pt bonds and thereby increases the ORR activity [12,32]. Such a mechanism may be operative in the present system. However, as shown below, the loss in ECSA of Pt<sub>ML</sub>PdNiN/C is much smaller than that of Pt<sub>ML</sub>Pd/C, presumably because the presence of nitride phase retards the dissolution rate.

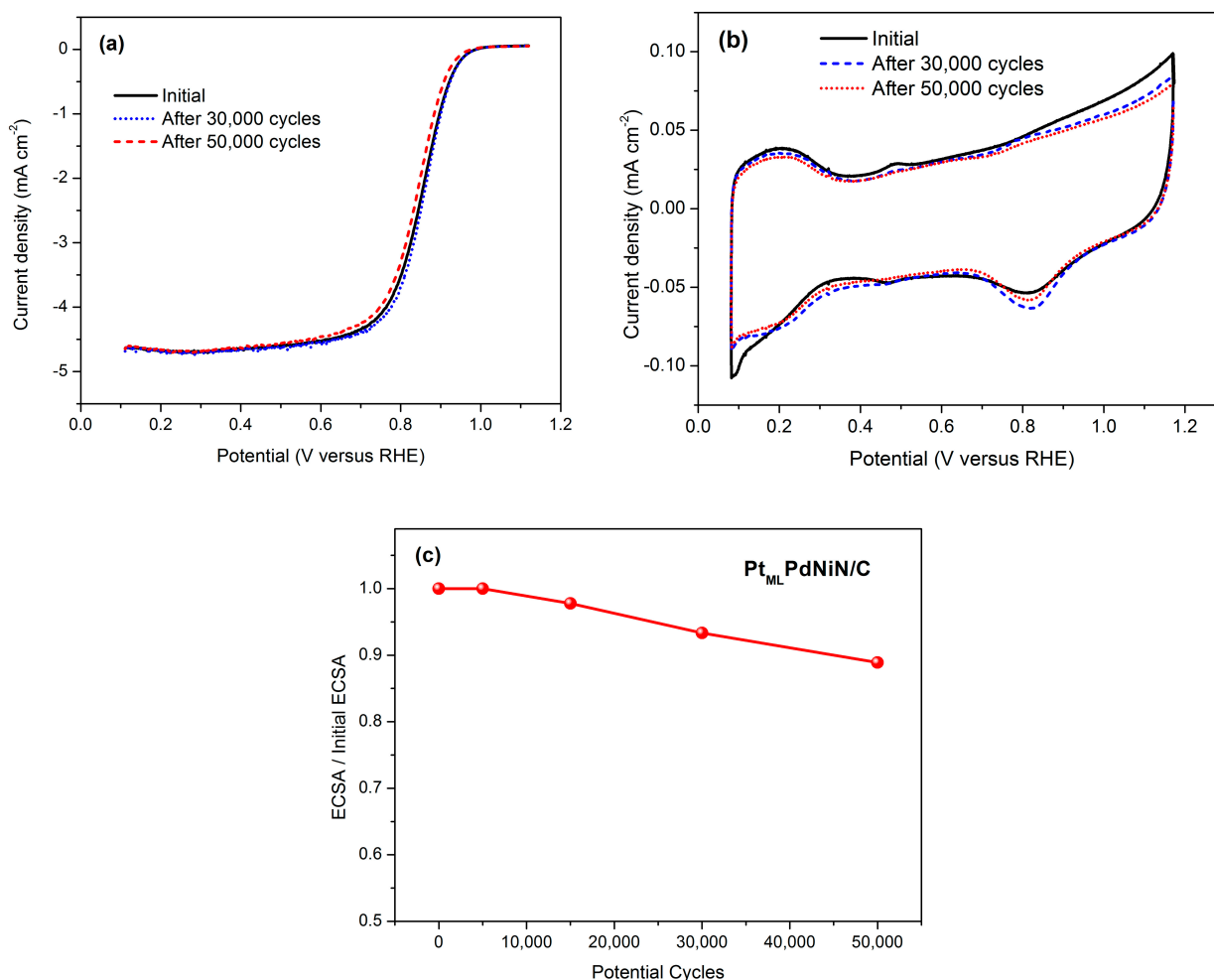


**Figure 5.** (a) ORR polarization curves and (b) cyclic voltammograms of the obtained Pt<sub>ML</sub>PdNiN/C catalyst before and after 50,000 cycles test between 0.6 and 1.0 V in 0.1 M HClO<sub>4</sub> solution; (c) ECSA degradation for Pt<sub>ML</sub>PdNiN/C catalyst plotted as a function of the number of after potential cycles between 0.6 and 1.0 V.

Figure 5b shows the CV curves of the Pt<sub>ML</sub>PdNiN/C catalyst in 0.1 M HClO<sub>4</sub> solution before and after cycling indicating a negligible loss of Pt surface area. The ECSA losses of the Pt<sub>ML</sub>PdNiN/C catalyst after different cycles are shown in Figure 5c. As reported in our previous paper, the Pt<sub>ML</sub>Pd/C catalyst exhibited a drastic decrease in ECSA after electrochemical cycling (27% after 5000 cycles and 34% after 15,000 cycles) due to the dissolution of Pd from the core [21]. Incorporation of Ni in the Pd core can slow down the Pd dissolution and as a result decrease the ECSA loss to 11.5% after 5000 cycles.

But further cycling of the PdNi core leads to an ECSA loss of 28% after 15,000 cycles. Nitriding the PdNi core restrains the dissolution process, the ECSA loss of the Pt<sub>ML</sub>PdNiN/C catalyst, as shown in Figure 5c, is only 11% after 50,000 cycles. By further comparing to the commercial Pt/C catalyst which only retains 55% of its initial ECSA after 30,000 cycles, the less ECSA loss of the obtained Pt<sub>ML</sub>PdNiN/C catalyst indicates that stabilization in the metal core by nitrogen modification exhibits a significant improvement in Pt stability [19]. ORR activities of the Pt<sub>ML</sub>PdNiN/C catalyst before and after an accelerated durability test are listed in Table 1.

**Table 1.** Catalytic activities of the Pt<sub>ML</sub>PdNiN/C catalyst before and after the accelerated durability test.

| Pt <sub>ML</sub> PdNiN/C | ECSA (m <sup>2</sup> ·g <sup>-1</sup> Pt) | E <sub>1/2</sub> (mV) | Specific activity (mA·cm <sup>-2</sup> ) | Pt mass activity (A·mg <sup>-1</sup> ) |
|--------------------------|---|-----------------------|--|--|
| Initial                  | 90  | 850                   | 1.17                                     | 1.05                                   |
| After 30,000 cycles      | 84  | 854                   | 1.35                                     | 1.13                                   |
| After 50,000 cycles      | 80  | 840                   | 0.84                                     | 0.67                                   |

### 3. Experimental Section

#### 3.1. Preparation of PdNiN/C Nanoparticles

PdNi nanoparticles were synthesized by mixing a 1:1 molar ratio of Pd(NO<sub>3</sub>)<sub>2</sub>·H<sub>2</sub>O (Sigma-Aldrich, St. Louis, MO, USA) and Ni(HCO<sub>2</sub>)<sub>2</sub>·2H<sub>2</sub>O (Sigma-Aldrich) salts with high area Vulcan XC-72R carbon black in MilliQ UV-plus water (Millipore corporation, Billerica, MA, USA) to obtain a total metal loading of 20 wt %. After sonicating the mixture for an hour under continuous Ar flow, NaBH<sub>4</sub> (Sigma-Aldrich) was added into the mixture and was then kept under sonication for 1 h. The mixture was filtered and rinsed with MilliQ UV-plus water (Millipore corporation), and then dried. The obtained PdNi/C nanoparticles were annealed in N<sub>2</sub> at 250 °C for 1 h followed by annealing at 510 °C for 2 h using NH<sub>3</sub> as the nitrogen precursor to get the PdNiN/C nanoparticles.

#### 3.2. Characterization

The microstructure of the synthesized PdNiN/C nanoparticles was characterized by HD-2700C aberration-corrected STEM (Hitachi, Clarksburg, MD, USA) using a 1.4 Å electron probe with probe current ~50 pA and an energy resolution of 0.35 eV, at the Center for Functional Nanomaterials (CFN), Brookhaven National Laboratory (BNL). Elementary sensitive EELS line scan and mapping were carried out for Pd M-edge (2122 eV), Ni L-edge (855 eV) across various single PdNiN/C nanoparticle. The XAS measurements were undertaken at the National Synchrotron Light Source, BNL (Upton, NY, USA) using Beam Line X19A. The content of Pd and Ni in the PdNiN/C, measured by inductively coupled plasma-optical emission spectrometry (ICP-OES), were 8.2 wt % and 7.0 wt % respectively.

#### 3.3. Electrochemical Measurements

Electrochemical testing was carried out in a three-electrode test cell by using a potentiostat (CHI 700B, CH Instruments, Austin, TX, USA). Before testing, catalyst ink was prepared by ultrasonic mixing of 5 mg of catalyst with 5 mL Millipore water until a dark and uniform aqueous dispersion was

achieved. A thin film of the catalyst was prepared on a glassy carbon RDE with the area of 0.196 cm<sup>2</sup> by placing 10–15 μL of the obtained dispersion and then covered by a 10 μL dilute Nafion solution (2 μg·μL<sup>-1</sup>). We deposited Pt monolayer both on the prepared PdNiN/C nanoparticle and commercial Pd/C nanoparticle surfaces using the galvanic displacement of Cu monolayer formed by Cu under-potential deposition (UPD) [6,16]. The Pt loadings on the RDE for the Pt<sub>ML</sub>PdNiN/C and Pt<sub>ML</sub>Pd/C catalysts were 1.13 and 3.75 μg·cm<sup>-2</sup> respectively whereas their Pd loadings were 0.82 and 2.0 μg·cm<sup>-2</sup> respectively. However, we note that a catalyst with higher loadings would be required for MEA preparation (future work) to replicate the ORR activity as that of RDE. The Pt loading on RDE for the commercial Pt/C catalyst was 7.65 μg·cm<sup>-2</sup>. The electrochemical measurements were all performed at room temperature, and the potentials were referenced to that of the reversible hydrogen electrode (RHE).

#### 4. Conclusions

We described a promising route to develop nitride-stabilized substrates for Pt monolayer catalyst with substantial reduction in platinum group metal loading while retaining high ORR activity and stability. Using STEM-EELS mapping techniques we have investigated the core-shell structure of the catalyst while XAS measurement emphasized the NiN<sub>x</sub> species in the core of the nanoparticles providing a stable support for Pt monolayer electrocatalysts.

#### Acknowledgments

This manuscript has been authored by employees of Brookhaven Science Associates, LLC under Contract No. DE-SC0012704 with the U.S. Department of Energy. The publisher by accepting the manuscript for publication acknowledges that the United States Government retains a non-exclusive, paid-up, irrevocable, world-wide license to publish or reproduce the published form of this manuscript, or allow others to do so, for United States Government purposes. This research used electron microscopy facility of the Center for Functional Nanomaterials, which is a U.S. DOE Office of Science Facility, at Brookhaven National Laboratory. Beam lines X19A at the National Synchrotron Light Source are supported in part by the Synchrotron Catalysis Consortium, U.S. Department of Energy Grant No DE-FG02-05ER15688. This work was also conducted under the framework of KIER's (Korea Institute of Energy Research) Research and Development Program (B5-2425).

#### Author Contributions

R.R.A., K.S. conceived and designed the experiments; K.A.K. performed the experiments; K.A.K. and J.H. analyzed the data and co-wrote the manuscript; D.S. performed the STEM-EELS analysis; K.S. and K.A.K. performed the XAS analysis; All authors contributed to the manuscript and the interpretation of the results.

#### Conflicts of Interest

The authors declare no conflict of interest.

## References

1. Borup, R.; Meyers, J.; Pivovarov, B.; Kim, Y.S.; Mukundan, R.; Garland, N.; Myers, D.; Wilson, M.; Garzon, F.; Wood, D.; *et al.* Scientific Aspects of Polymer Electrolyte Fuel Cell Durability and Degradation. *Chem. Rev.* **2007**, *107*, 3904–3951.
2. Jacobson, M.Z.; Colella, W.G.; Golden, D.M. Cleaning the Air and Improving Health with Hydrogen Fuel-Cell vehicles. *Science* **2005**, *308*, 1901–1905.
3. Gasteiger, H.A.; Markovic, N.M. Just a Dream-or Future Reality? *Science* **2009**, *324*, 48–49.
4. Debe, M.K. Electrocatalyst Approaches and Challenges for Automotive Fuel Cells. *Nature* **2012**, *486*, 43–51.
5. Yasuda, K.; Taniguchi, A.; Akita, T.; Ioroi, T.; Siroma, Z. Platinum Dissolution and Deposition in the Polymer Electrolyte Membrane of a PEM Fuel Cell as Studied by Potential Cycling. *Phys. Chem. Chem. Phys.* **2006**, *8*, 746–752.
6. Adzic, R.R.; Zhang, J.; Sasaki, K.; Vukmirovic, M.B.; Shao, M.; Wang, J.X.; Nilekar, A.U.; Mavrikakis, M.; Valerio, J.A.; Uribe, F. Platinum Monolayer Fuel Cell Electrocatalysts. *Top. Catal.* **2007**, *46*, 249–262.
7. Shao, M.; Shoemaker, K.; Peles, A.; Kaneko, K.; Protsailo, L. Pt Monolayer on Porous Pd-Cu Alloys as Oxygen Reduction Electrocatalysts. *J. Am. Chem. Soc.* **2010**, *132*, 9253–9255.
8. Strasser, P.; Koh, S.; Anniyev, T.; Greeley, J.; More, K.; Yu, C.F.; Liu, Z.C.; Kaya, S.; Nordlund, D.; Ogasawara, H.; *et al.* Lattice-strain control of the activity in dealloyed core-shell fuel cell catalysts. *Nat. Chem.* **2010**, *2*, 454–460.
9. Wang, D.L.; Xin, H.L.L.; Hovden, R.; Wang, H.S.; Yu, Y.C.; Muller, D.A.; DiSalvo, F.J.; Abruna, H.D. Structurally ordered intermetallic platinum-cobalt core-shell nanoparticles with enhanced activity and stability as oxygen reduction electrocatalysts. *Nat. Mater.* **2013**, *12*, 81–87.
10. Brimaud, S.; Behm, R.J. Electrodeposition of a Pt Monolayer Film: Using Kinetic Limitations for Atomic Layer Epitaxy. *J. Am. Chem. Soc.* **2013**, *135*, 11716–11719.
11. Zhao, X.; Chen, S.; Fang, Z.; Ding, J.; Sang, W.; Wang, Y.; Zhao, J.; Peng, Z.; Zeng, J. Octahedral Pd@Pt<sub>1.8</sub>Ni Core-Shell Nanocrystals with Ultrathin PtNi Alloy Shells as Active Catalysts for Oxygen Reduction Reaction. *J. Am. Chem. Soc.* **2015**, *137*, 2804–2807.
12. Wang, J.X.; Inada, H.; Wu, L.J.; Zhu, Y.M.; Choi, Y.M.; Liu, P.; Zhou, W.P.; Adzic, R.R. Oxygen Reduction on Well-Defined Core-Shell Nanocatalysts: Particle Size, Facet, and Pt Shell Thickness Effects. *J. Am. Chem. Soc.* **2009**, *131*, 17298–17302.
13. Karan, H.I.; Sasaki, K.; Kuttiyiel, K.; Farberow, C.A.; Mavrikakis, M.; Adzic, R.R. Catalytic Activity of Platinum Monolayer on Iridium and Rhenium Alloy Nanoparticles for the Oxygen Reduction Reaction. *ACS Catal.* **2012**, *2*, 817–824.
14. Zhang, Y.; Hsieh, Y.C.; Volkov, V.; Su, D.; An, W.; Si, R.; Zhu, Y.M.; Liu, P.; Wang, J.X.; Adzic, R.R. High Performance Pt Monolayer Catalysts Produced via Core-Catalyzed Coating in Ethanol. *ACS Catal.* **2014**, *4*, 738–742.
15. Zhang, Y.; Ma, C.; Zhu, Y.M.; Si, R.; Cai, Y.; Wang, J.X.; Adzic, R.R. Hollow core supported Pt monolayer catalysts for oxygen reduction. *Catal. Today* **2013**, *202*, 50–54.

16. Kuttiyiel, K.A.; Sasaki, K.; Choi, Y.; Su, D.; Liu, P.; Adzic, R.R. Bimetallic IrNi Core Platinum Monolayer Shell Electrocatalysts for the Oxygen Reduction Reaction. *Energy Environ. Sci.* **2012**, *5*, 5297–5304.
17. Hsieh, Y.-C.; Zhang, Y.; Su, D.; Volkov, V.; Si, R.; Wu, L.; Zhu, Y.; An, W.; Liu, P.; He, P.; *et al.* Ordered Bilayer Ruthenium-Platinum Core-Shell Nanoparticles as Carbon Monoxide-Tolerant Fuel Cell Catalysts. *Nat. Commun.* **2013**, *4*, 1–9.
18. Zhang, J.; Vukmirovic, M.B.; Xu, Y.; Mavrikakis, M.; Adzic, R.R. Controlling the Catalytic Activity of Platinum-Monolayer Electrocatalysts for Oxygen Reduction with Different Substrates. *Angew. Chem. Int. Ed.* **2005**, *44*, 2132–2135.
19. Zhang, J.; Sasaki, K.; Sutter, E.; Adzic, R.R. Stabilization of Platinum Oxygen-Reduction Electrocatalysts Using Gold Clusters. *Science* **2007**, *315*, 220–222.
20. Gong, K.; Su, D.; Adzic, R.R. Platinum-Monolayer Shell on AuNi<sub>0.5</sub>Fe Nanoparticle Core Electrocatalyst with High Activity and Stability for the Oxygen Reduction Reaction. *J. Am. Chem. Soc.* **2010**, *132*, 14364–14366.
21. Kuttiyiel, K.A.; Sasaki, K.; Su, D.; Vukmirovic, M.B.; Marinkovic, N.S.; Adzic, R.R. Pt monolayer on Au-Stabilized PdNi Core-Shell Nanoparticles for Oxygen Reduction Reaction. *Electrochim. Acta* **2013**, *110*, 267–272.
22. Kuttiyiel, K.A.; Sasaki, K.; Choi, Y.M.; Su, D.; Liu, P.; Adzic, R.R. Nitride Stabilized PtNi Core-Shell Nanocatalyst for High Oxygen Reduction Activity. *Nano Lett.* **2012**, *12*, 6266–6271.
23. Kuttiyiel, K.A.; Choi, Y.; Hwang, S.-M.; Park, G.-G.; Yang, T.-H.; Su, D.; Sasaki, K.; Liu, P.; Adzic, R.R. Enhancement of the Oxygen Reduction on Nitride Stabilized Pt–M (M = Fe, Co, and Ni) Core-Shell Nanoparticle Electrocatalysts. *Nano Energy* **2015**, *13*, 442–449.
24. Liu, H.; Koenigsmann, C.; Adzic, R.R.; Wong, S.S. Probing Ultrathin One-Dimensional Pd–Ni Nanostructures As Oxygen Reduction Reaction Catalysts. *ACS Catal.* **2014**, *4*, 2544–2555.
25. Subbaraman, R.; Tripkovic, D.; Strmcnik, D.; Chang, K.-C.; Uchimura, M.; Paulikas, A.P.; Stamenkovic, V.; Markovic, N.M. Enhancing Hydrogen Evolution Activity in Water Splitting by Tailoring Li<sup>+</sup>-Ni(OH)<sub>2</sub>-Pt Interfaces. *Science* **2011**, *334*, 1256–1260.
26. Chu, Y.-Y.; Wang, Z.-B.; Gu, D.-M.; Yin, G.-P. Performance of Pt/C catalysts prepared by microwave-assisted polyol process for methanol electrooxidation. *J. Power Sources* **2010**, *195*, 1799–1804.
27. Schmidt, T.J.; Gasteiger, H.A.; Stäb, G.D.; Urban, P.M.; Kolb, D.M.; Behm, R.J. Characterization of High-Surface-Area Electrocatalysts Using a Rotating Disk Electrode Configuration. *J. Electrochem. Soc.* **1998**, *145*, 2354–2358.
28. Sasaki, K.; Wang, J.X.; Naohara, H.; Marinkovic, N.; More, K.; Inada, H.; Adzic, R.R. Recent Advances in Platinum Monolayer Electrocatalysts for Oxygen Reduction Reaction: Scale-up Synthesis, Structure and Activity of Pt Shells on Pd Cores. *Electrochim. Acta* **2010**, *55*, 2645–2652.
29. Garsany, Y.; Singer, I.L.; Swider-Lyons, K.E. Impact of film drying procedures on RDE characterization of Pt/VC electrocatalysts. *J. Electroanal. Chem.* **2011**, *662*, 396–406.
30. Takahashi, I.; Kocha, S.S. Examination of the activity and durability of PEMFC catalysts in liquid electrolytes. *J. Power Sources* **2010**, *195*, 6312–6322.

31. Sasaki, K.; Naohara, H.; Cai, Y.; Choi, Y.M.; Liu, P.; Vukmirovic, M.B.; Wang, J.X.; Adzic, R.R. Core-Protected Platinum Monolayer Shell High-Stability Electrocatalysts for Fuel-Cell Cathodes. *Angew. Chem. Int. Ed.* **2010**, *49*, 8602–8607.
32. Wang, J.X.; Ma, C.; Choi, Y.M.; Su, D.; Zhu, Y.M.; Liu, P.; Si, R.; Vukmirovic, M.B.; Zhang, Y.; Adzic, R.R. Kirkendall Effect and Lattice Contraction in Nanocatalysts: A New Strategy to Enhance Sustainable Activity. *J. Am. Chem. Soc.* **2011**, *133*, 13551–13557.

© 2015 by the authors; licensee MDPI, Basel, Switzerland. This article is an open access article distributed under the terms and conditions of the Creative Commons Attribution license (<http://creativecommons.org/licenses/by/4.0/>).